Title

Monitoring protein assembly using quasielastic light scattering spectroscopy.

Journal

Methods in enzymology, 309

ISSN

0076-6879

Authors

Lomakin, A
Benedek, GB
Teplow, DB

Publication Date

1999

DOI

10.1016/s0076-6879(99)09029-1

Peer reviewed

quenchers is also affected by electrostatic interactions. Collisional quenching of fluorescence is described by the Stern–Volmer equation:

$$F_o/F = 1 + K[Q] \quad (10)$$

where F_o and F are the fluorescence intensities in the absence and presence of quencher, respectively, Q is the concentration of the quencher, and K the Stern–Volmer quenching constant. By plotting the ratio F_o/F against the concentration of the quencher, a linear relation should be obtained for collisional quenching, and the Stern–Volmer quenching constant, K, indicates how accessible the fluorophore is. The quenching experiment is performed by injecting buffer solutions with increasing concentrations of the quencher while measuring the fluorescence intensity at the maximum emission wavelength. The adsorbed protein quenching is compared with the quenching of the same protein in bulk solution or at some other standard conditions. As desorption of proteins from the surface might occur, the fluorescence intensity of the sample without the presence of a quencher in the buffer solution is measured between the quenched fluorescence intensity measurements.

[27] Monitoring Protein Assembly Using Quasielastic Light Scattering Spectroscopy

By ALEKSEY LOMAKIN, GEORGE B. BENEDEK, and DAVID B. TEPLOW

Introduction

The process of protein assembly is vital for the survival of all organisms, from those as complex as humans to those as simple as viruses. Common macromolecular assembly reactions include actin and tubulin polymerization, collagen and myosin fibrillization, and formation of bacterial flagella and viral capsids. Ordered protein assembly is also required to produce multisubunit structures with enzymatic, transport, or other activities, such as bacterial aspartate transcarbamoylase, ribosomes, proteasomes, ion channels, receptor complexes, and transcription complexes.

In addition to their role in the normal physiology of living organisms, protein assembly reactions have been found to be associated with, or causative of, an increasing number of human diseases. Examples include Alzheimer's disease,[1] prion diseases,[2] and a large variety of systemic amy-

[1] D. J. Selkoe, *J. Neuropathol. Exp. Neurol.* **53,** 438 (1994).
[2] A. L. Horwich and J. S. Weissman, *Cell* **89,** 499 (1997).

0076-6879/99 $30.00

loidoses.[3] In each case, proteins that exist normally in a soluble, disaggregated state assemble into ordered polymers, which then form insoluble deposits. Because the proteins involved participate in normal physiologic processes, therapeutic strategies targeting their production may be unfeasible. Therefore, efforts have been directed at inhibiting and/or reversing the aberrant assembly and deposition of these proteins. To achieve this goal, the key factors controlling the assembly process must be elucidated. This requires both model systems in which reproducible and experimentally manipulable protein assembly occurs and the ability to monitor the process with high sensitivity and resolution. This article discusses the use of quasielastic light scattering spectroscopy (QLS)[4] for monitoring protein assembly reactions.

QLS is an optical method for the determination of diffusion coefficients of particles undergoing Brownian motion in solution.[5,6] Knowledge of diffusion coefficients allows one to determine many features of the molecules under study, including their size, shape, and flexibility. Temporal changes in these parameters provide important information about the kinetics and structural transitions that occur during protein assembly. The QLS method is rapid, sensitive, noninvasive, and quantitative, which makes it useful for thermodynamic studies. Although QLS spectrometers may be constructed relatively easily and are also available commercially, obtaining accurate and meaningful information from a QLS experiment requires thorough knowledge of the theoretical and practical aspects of the technique. This point cannot be overemphasized.

"Quick Start" Guide for the Reader

The first three sections of this article address the theoretical underpinnings of the QLS method and include general discussions of experimental techniques of light scattering, of quasielastic light scattering from macromolecules in solution, and of methods of analyzing QLS data. Next are presented sections on unique features of the QLS monitoring of fibril growth and important practical considerations in the execution of the QLS experiment. Finally, a number of real-world examples of QLS studies of amyloid β-protein (Aβ) fibril formation are presented. Those readers already con-

[3] P. Westermark, *Am. J. Pathol.* **152,** 1125 (1998).

[4] The method of QLS is also referred to as "dynamic light scattering" and "photon correlation spectroscopy." These, and several other terms, are interchangeable.

[5] R. Pecora, "Dynamic Light Scattering: Applications of Photon Correlation Spectroscopy." Plenum Press, New York, 1985.

[6] K. S. Schmitz, "An Introduction to Dynamic Light Scattering by Macromolecules." Academic Press, Boston, 1990.

versant in the theory of QLS or who may wish to simply understand the types of data obtainable using the method are encouraged to focus first on the last section of the article and then, if desired, to examine the penultimate two sections on unique and practical aspects of QLS studies of fibrillogenesis. For those readers new to the QLS method or interested in applying the method in their own laboratories, starting at the beginning is highly recommended.

General Principles

Light Scattering

The propagation of light may be viewed as a continuous rescattering of the incident electromagnetic wave from every point of the illuminated medium. The amplitude of each secondary wave is proportional to the polarizability at the point from which this wave originates. If the medium is uniform, rescattered waves all have the same amplitude and interfere destructively in all directions except in the direction of the incident beam. If, however, at some location the index of refraction differs from its average value, the wave rescattered at this location is not compensated for and some light can be observed in directions other than the direction of incidence, i.e., light scattering occurs. The scattering of light may thus be viewed as a result of microscopic heterogeneities within the illuminated volume. Macromolecules and supramolecular assemblies are examples of such heterogeneities.

Light-Scattering Techniques

Light scattering is a versatile approach for noninvasive, fast, and accurate study of scattering media. The simplest light scattering technique is turbidimetry. Turbidimetry measures attenuation in the intensity of light as it passes through a scattering medium. This attenuation is characterized quantitatively by the extinction coefficient, which is determined by the concentration, molecular weight, and size of the scatterers. Turbidity is a good indicator of phenomena such as aggregation, agglutination or phase separation, in which large scatterers alter the macroscopic properties of the medium. It is widely used to detect and monitor formation and subsequent aggregation of Aβ fibrils.

Static light scattering probes concentration, molecular weight, size, shape, orientation, and interactions among scattering particles by measuring the average intensity and polarization of the scattered light. Static light scattering measurements done at different scattering angles provide infor-

mation on the molecular weight, size, and shape of the scattering particles. Measurements of the intensity of light scattering as a function of concentration yield the second virial coefficient, which is the key characteristic of the strength of attractive or repulsive interactions between solute particles.

Quasielastic light scattering probes the relatively slow fluctuations in concentration, shape, orientation, and other particle characteristics by measuring the correlation function of the scattered light intensity. Fast vibrations of small chemical groups, which lead to significant changes in the frequency of the scattered light, are the domain of Raman spectroscopy. These latter two methods, which probe the dynamics of the scatterers, are intrinsically more complicated than static light scattering, as they involve measurements of spectral characteristics or related correlation properties of the scattered light.

The spectrum of the scattered light is affected by the motion of the scattered particles. Fast motion leads to large changes, which can be measured using classical interferometers. The slow motion associated with the diffusion of macromolecules in solution leads to tiny changes in the frequency of the scattered light. Only with the advent of lasers has it become practical to observe these small spectral changes indirectly by measuring the correlation function of the scattered light intensity, i.e., by QLS.

Light Scattering from Macromolecules in Solution

In solutions there are two equivalent ways to describe light scattering. One way is to consider the solution as a homogeneous medium and ascribe light scattering to the spatial fluctuations in the concentration of a solute. An alternative way is to consider each individual solute particle as a heterogeneity and therefore as a source of light scattering. The first approach is more appropriate for solutions of small molecules in which the average distance between scatterer centers is small compared to the wavelength of light. The second approach is more appropriate for solutions of large macromolecules and colloids, when the average distance between particle centers is comparable to the wavelength of light. In the case of amyloid fibrils, the size of the solute particles themselves becomes comparable to the wavelength of light. In this case, the description of the effects of orientational motion and deformation of the solute particles is much more straightforward when these particles are treated as individual scatterers.

Using these considerations, we will describe light scattering in a solution of macromolecules as a result of the interference of electromagnetic waves scattered by individual solute particles with a refractive index not matching that of the solvent. Thus, the first question to address is the intensity of the light scattered by a single particle and its dependence on the mass and

the shape of the particle. We first consider an aggregate composed of m monomers. Let the amplitude of the electromagnetic wave scattered by an individual monomer be E_0 (at the point of observation). If the size of the aggregate is small compared to the wavelength of light, λ, all waves scattered by individual monomers interfere constructively and the resulting wave has an amplitude $E = mE_0$. The intensity of a light wave is proportional to its amplitude squared. Thus the intensity of the light scattered by the aggregate is proportional to the aggregation number squared, $I = m^2 I_0$, where I_0 is the intensity of scattering by a monomer. The quadratic dependency of scattering intensity on the size of the scatterer is the basis for optical determination of the molecular weight of macromolecules, for various turbidimetry techniques, and for understanding many natural phenomena, from critical opacification to cataractogenesis in the eye lens.[7]

If an aggregate particle is not small compared to λ, the interference of the electromagnetic waves scattered by the constituent monomers is not all constructive and the phases of these waves must be taken into account. If the phase of a wave scattered at the origin is used as a reference, the phase of a wave scattered at a point with radius vector $\mathbf{r}$ is $\mathbf{q} \cdot \mathbf{r}$ (Fig. 1). The vector $\mathbf{q}$ is called the "scattering vector" and is a fundamental characteristic of any scattering process. Its length is $q \equiv |\mathbf{q}| = 4\pi n/\lambda \cdot \sin \theta/2$, where n is the refractive index of the medium, λ is the wavelength of light, and θ is the scattering angle. Partial cancellation of waves scattered by different parts of the large aggregate reduces the intensity of light scattering by a factor of $|\alpha|^2$, where α is an averaged value of the phase factors $\exp(i\mathbf{q} \cdot \mathbf{r})$ for all monomers. The factor α should be averaged over all possible orientations of the particle. The result of this averaging yields the structure factor, $S(q)$. Expressions for the structure factors for particles of various shapes can be found elsewhere.[8]

Method of Quasielastic Light Scattering Spectroscopy

Motion of Particles in Solution Causes Temporal Fluctuations in Scattered Light Intensity

We are now in a position to analyze the light scattered from a collection of N solute molecules. For the moment, we will assume that the solution is sufficiently dilute so that the scattering particles move independently. At the observation point we again have a sum of waves scattered by individual particles, but this time each particle could be at any random location within

[7] G. B. Benedek, *Appl. Opt.* **10,** 459 (1971).
[8] H. C. van de Hulst, "Light Scattering by Small Particles." Dover, New York, 1981.

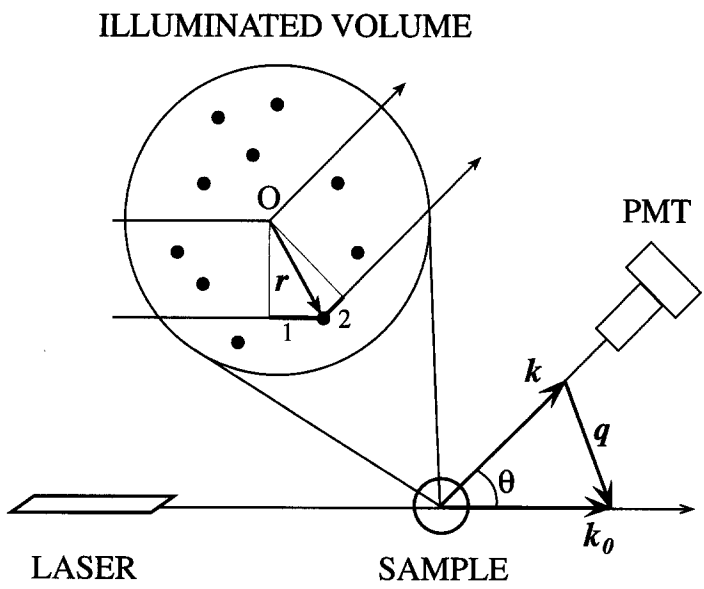

FIG. 1. The scattering vector **q**. The path traveled by a wave scattered at the point with radius vector **r** differs from the path passing through the reference point O by two segments, 1 and 2, with lengths l_1 and l_2, respectively. The phase difference is $\Delta\phi = k(l_1 + l_2)$, where $k \equiv |\mathbf{k}| = |\mathbf{k}_0| = 2\pi n/\lambda$ is the absolute value of the wave vector **k** (or $\mathbf{k}_0$). The segment l_1 is a projection of **r** on the wave vector of the incident beam $\mathbf{k}_0$, i.e., $l_1 = \mathbf{r} \cdot \mathbf{k}_0/k$. Similarly, $l_2 = -\mathbf{r} \cdot \mathbf{k}/k$, and thus $\Delta\phi = \mathbf{r} \cdot (\mathbf{k}_0 - \mathbf{k}) = \mathbf{rq}$. Vector $\mathbf{q} = \mathbf{k}_0 - \mathbf{k}$ is called the scattering vector.

the scattering volume (the intersection of the illuminated volume and the volume from which the scattered light is collected). The size of the scattering volume is much bigger than q^{-1} (with the exception of nearly forward scattering, where $q \sim \theta \approx 0$) and the phases of the waves scattered by different particles vary dramatically. As a result, the average amplitude of the scattered wave is proportional to $N^{1/2}$. Thus the average intensity of the scattered light is simply N times the intensity scattered by an individual particle, as expected. The local intensity, however, fluctuates from one point to another around its average value. The spatial pattern of these fluctuations in light intensity, called an interference pattern or "speckles," is determined by the positions of the scattering particles. As the scattering particles move, the interference pattern changes in time, resulting in temporal fluctuations in the intensity of light detected at the observation point. The essence of the QLS technique is to measure the temporal correlations in the fluctuations in the scattered light intensity and to reconstruct the physical characteristics of the scatterers from these data.

Coherence Area

There is a characteristic size for speckles in the interference pattern. If the intensity of the scattered light is above average at a certain point it will also be above the average within an area around this point where phases of the scattered waves do not change significantly. This area is called the coherence area. Within different coherence areas, fluctuations in the intensity of light collected are statistically independent. Therefore, increasing the size of the light-collecting aperture in a QLS spectrometer beyond the size of a coherence area does not lead to improvement of the signal-to-noise ratio because the temporal fluctuations in the intensity are averaged out. For a monochromatic source, the scattered light is coherent within a solid angle of the order of λ^2/A, where A is the cross-sectional area of the scattered volume perpendicular to the direction of the scattering. Because the coherence angle is fairly small, powerful (10–500 mW) and well-focused laser illumination and photon-counting techniques are used in QLS.

Correlation Function

The photodetector signal in QLS is, in fact, random noise. Information is contained only in the spectrum or correlation function of this random signal (the spectrum is a Fourier transform of the correlation function). The correlation function of the signal $i(t)$, which in the particular case of QLS is the photocurrent, is defined as

$$G^{(2)}(\tau) = \langle i(t)i(t + \tau)\rangle \tag{1}$$

The notation $G^{(2)}(\tau)$ is introduced to distinguish the correlation function of the photocurrent from the correlation function of the electromagnetic field $G^{(1)}(\tau)$, which is the Fourier transform of the light spectrum:

$$G^{(1)}(\tau) = \langle E(t)E^*(t + \tau)\rangle \tag{2}$$

In Eqs. (1) and (2), angular brackets denote an average over time t. This time averaging, an inherent feature of the QLS method, is necessary to extract information from the random fluctuations in the intensity of the scattered light.

For very large delay times τ, the photocurrents at moment t and $t + \tau$ are completely uncorrelated and $G^{(2)}(\infty)$ is simply the square of the mean current $\bar{i}^2$. At $\tau = 0$, $G^{(2)}(0)$ is obviously the mean of the current squared $\overline{i^2}$. Since for any $i(t)$, $\overline{i^2} \geq \bar{i}^2$, the initial value of the correlation function is always larger than the value at a sufficiently long delay time. The characteristic time within which the correlation function approaches its final value is called correlation time. For example, in the most practically important

case of a correlation function that decays according to an exponential law $\exp(-\tau/\tau_c)$, the correlation time is the parameter τ_c.

In the majority of practical applications of QLS, the scattered light is a sum of waves scattered by many independent particles and therefore displays Gaussian statistics. This being the case, there is a relation between the intensity correlation function $G^{(2)}(\tau)$ and the field correlation function $G^{(1)}(\tau)$:

$$G^{(2)}(\tau) = I_0^2(1 + \gamma|g^{(1)}(\tau)|^2) \tag{3}$$

Here $g^{(1)}(\tau) \equiv G^{(1)}(\tau)/G^{(1)}(0)$ is the normalized field correlation function, I_0 is the average intensity of the detected light, and γ is the efficiency factor. For perfectly coherent incident light and for scattered light collected within one coherence area, the efficiency factor is 1. If light is collected from an area J times larger than the coherence area, fluctuations in light intensity are averaged out and the efficiency factor is of the order of $1/J \ll 1$. Low efficiency makes the quality of measurements extremely vulnerable to fluctuations in the average intensity caused by the presence of large dust particles in the sample or by instability of the laser intensity. It is thus highly desirable to collect the scattered light from within one coherence area. Unfortunately, this is not always possible because the coherence area is small and the intensity of light might be too low. If fewer than one photon is registered per correlation time τ_c, the statistical accuracy of the correlation function deteriorates rapidly. The optimal size of the light-collecting aperture thus varies depending on the conditions of the experiment.

Determination of Correlation Function

In modern instruments the correlation function is determined digitally. The number of photons registered by the photodetector within each of a number of short consecutive intervals is stored in the correlator memory. Each count in a given interval (termed the "sample time" and denoted Δt) represents the instantaneous value of the photocurrent $i(t)$. The series of K counts held in the correlator memory is termed the "digitized copy" of the signal. According to Eq. (1), to obtain the correlation function $G^{(2)}(\tau)$ at $\tau = n\Delta t (n = 1 \ldots K)$, the average product of counts separated by n sample times should be determined. The number n is referred to as a channel number. Up to K channels, in principle, can be measured simultaneously, but usually a smaller subset of M equidistant or logarithmically spaced channels is used. Clearly, the shortest delay time at which the correlation function is measured by the procedure described earlier is Δt (channel 1). The longest delay time cannot exceed the duration of the

digitized copy, $K\Delta t$. Thus, it is important that the correlation time τ_c fit into the interval $\Delta t \ll \tau_c \ll K\Delta t$. This condition determines the choice of the sample time for the particular measurement.

To increase the statistical accuracy with which the correlation function is determined, it is essential to maximize the number of count pairs whose products are averaged within the measurement time. If the correlation function is being measured in M channels simultaneously, ideally M products should be processed for each new count, i.e., during sample time Δt. The instrument capable of doing this is said to be working in the "real-time regime." The real-time regime means that the information contained in the signal is processed without loss. The minimal sample time Δt and the number of channels M capable of being processed in real time are the most critical characteristics of a correlator. Modern commercial correlators, with several hundred channels for different delay times, can work in real time at sample times as low as a fraction of a microsecond. This capability is sufficient to measure diffusion coefficients of the smallest macromolecules.

QLS System

A QLS system consists of four elements: the sample, the optical equipment, the correlator, and the data analysis software (Fig. 2). To obtain satisfactory results, all four elements must meet certain criteria. The correlator should work close to the real-time regime for sample times significantly shorter than the correlation times of the molecules under investigation. The optical setup should collect at least one photon per correlation time per coherence area. Because the hardware characteristics of most commercial instruments are fixed, the just-described requirements determine whether a particular particle system can be studied by QLS at all. Among the more well-known suppliers of research grade spectrometers are Brookhaven Instruments (Holtsville, NY), Malvern Instruments (Malvern, UK), ALV (Langen, Germany), and Otsuka Electronics (Shiga, Japan). Simple, basic instruments are manufactured by Precision Detectors (Franklin, MA) and Protein Solutions (Charlottesville, VA). If instrument performance is suitable for a particular study, the quality and reliability of the results will be determined by the other two elements of the QLS system, namely the sample and the data analysis software. The rest of this article focuses on these two elements of the QLS experiment and provides practical examples taken from studies of Aβ fibrillogenesis.

Brownian Motion

Temporal fluctuations in the intensity of the scattered light are caused by the Brownian motion of the scattering particles. The smaller these

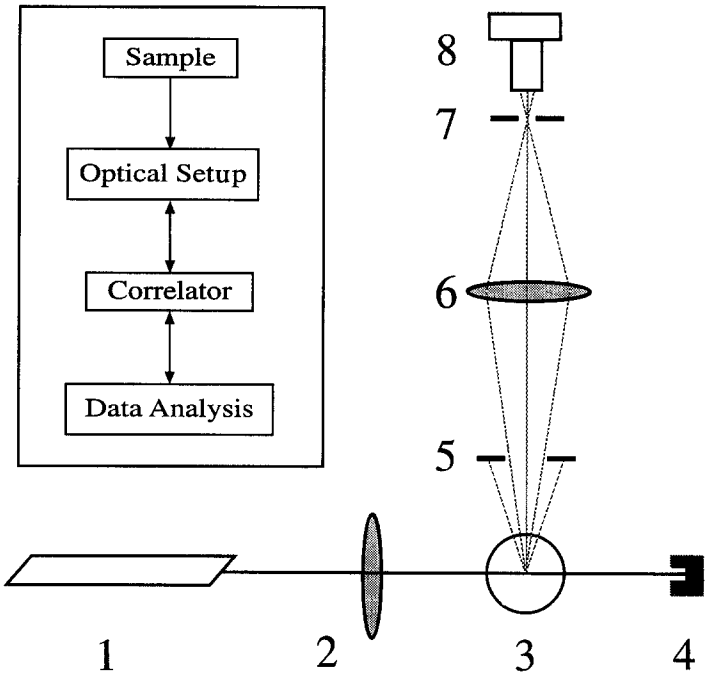

FIG. 2. A QLS instrument. The four key components of a QLS apparatus are presented in block diagram form within the box. Adjacent is a typical scheme for the optical arrangement of the spectrometer, which includes (1) laser; (2) focusing lens (to direct light to center of sample cuvette); (3) sample holder; (4) beam stop; (5) pinhole controlling the solid angle inside which the scattered light is collected; (6) focusing lens (to focus image of the beam within sample on pinhole 7); (7) pinhole, which determines the volume from which the scattered light is registered by photodetector; and (8) photodetector.

particles are, the faster they move. Although each particle moves randomly, in a unit time more particles leave regions of high concentration than leave regions of low concentration. This results in a net flux of particles along the concentration gradient. Brownian motion is thus responsible for the diffusion of the solute and is characterized quantitatively by the diffusion coefficient, D. The laws of diffusive motion stipulate that over time δt the displacement Δx of a Brownian particle in a given direction is characterized by the relationship $\overline{\Delta x^2} = 2D\delta t$.

Determination of Diffusion Coefficient D

As explained earlier, temporal fluctuations in scattered light intensity are caused by the relative motions of particles in solution. Two spherical waves scattered by a pair of individual particles have, at the observation

point, a phase difference of $\mathbf{q} \cdot \mathbf{r}$, where $\mathbf{r}$ is the (vector) distance between particles. As the scattering particles move over distance $\Delta x \approx q^{-1}$ along the vector $\mathbf{q}$, phases for all pairs of particles change significantly and the intensity of the scattered light becomes completely independent of its initial value. The correlation time, τ_c, is thus the time required for a Brownian particle to move a distance q^{-1} along the vector $\mathbf{q}$. As stated earlier $\overline{\Delta x^2} = 2D\delta t$, thus for $\Delta x \approx q^{-1}$, $\tau_c \sim 1/Dq^2$. Rigorous mathematical analysis of the process of light scattering by Brownian particles leads to the following expression for the correlation function of the scattered light:

$$|g^{(1)}(\tau)| = \exp(-Dq^2\tau) \tag{4}$$

Determination of Sizes of Particles in Solution

According to Eqs. (3) and (4), measurement of the intensity correlation function allows evaluation of the diffusion coefficients of the scattering particles. The diffusion coefficient in an infinitely dilute solution is determined by particle geometry. For spherical particles, the relation between the radius R and its diffusion coefficient D is given by the Stokes–Einstein equation:

$$D = \frac{k_B T}{6\pi\eta R} \tag{5}$$

Here k_B is the Boltzmann constant, T is the absolute temperature, and η is solution viscosity. For nonspherical particles it is customary to introduce the apparent hydrodynamic radius R_h^{app}, defined as:

$$R_h^{app} = \frac{k_B T}{6\pi\eta D^{app}} \tag{6}$$

where D^{app} is the diffusion coefficient measured in the QLS experiment.

For nonspherical particles, it is important to note that the diffusion coefficient is actually a tensor—the rate of particle diffusion in a certain direction depends on the particle orientation relative to this direction. Small particles, as they diffuse over a distance q^{-1}, change their orientation many times. QLS measures the average diffusion coefficient for these particles. Particles of a size comparable to, or larger than, q^{-1} essentially preserve their orientation as they travel a distance smaller than their size. For these particles, the single exponential expression of Eq. (4) for the field correlation function is not strictly applicable. This fact is particularly important in QLS applications designed for studying long fibrils and will be discussed in more detail later.

For particles small compared to q^{-1}, the hydrodynamic radius is calculated numerically, and in some cases analytically, for a variety of particles shapes. In studies of fibrils, the important analytical formula is that for the prolate ellipsoid, where a is long axis length and p is the ratio of lengths of the short axis to the long axis:

$$R_h = \frac{a}{2}\sqrt{1-p^2} \Big/ \ln\frac{1+\sqrt{1-p^2}}{p} \tag{7}$$

The numerical expression for the hydrodynamic radius of a long cylinder can be found in de la Torre and Bloomfield.[9] Effects of flexibility are discussed in the monograph by Schmitz.[6] For thin, rigid objects of length L short compared to q^{-1}, the following asymptotic form of Eq. (7) is useful, where d is the particle diameter:

$$R_h^{app} = \frac{L}{2\ln(2L/d)} \tag{8}$$

All of the formulas connecting the diffusion coefficient or hydrodynamic radius to particle geometry are strictly applicable only for infinitely dilute solutions. At finite concentrations, two additional factors affect the diffusion of particles significantly: viscosity and interparticle interactions. Viscosity generally increases with the concentration of macromolecular solute. According to Eq. (5), this leads to a lower diffusion coefficient and therefore to an increase in the apparent hydrodynamic radius. Interactions between particles can act in either direction. If the effective interaction is repulsive, which is usually the case for soluble molecules (otherwise they would not be soluble), local fluctuations in concentration tend to dissipate faster, meaning higher apparent diffusion coefficients and lower apparent hydrodynamic radii. If the interaction is attractive, fluctuations in concentration dissipate slower and the apparent diffusion coefficients are lower. Thus, depending on whether the effect of repulsion between particles is strong enough to overcome the effect of increased viscosity, both increasing and decreasing types of concentration dependence of the hydrodynamic radius are observed.[10] In this context, it should be noted that the interaction between large particles (as compared to q^{-1}) generally leads to a nonexponential correlation function that does not take the form of Eq. (4) and therefore cannot be described completely by a single parameter D^{app}.

[9] J. G. de la Torre and V. A. Bloomfield, *Quart. Rev. Biophys.* **14,** 81 (1981).
[10] M. Muschol and F. Rosenberger, *J. Chem. Phys.* **103,** 10424 (1995).

Data Analysis

Polydispersity and Mathematical Analysis of QLS Data

Polydisersity can be an inherent property of the sample, for instance when polymer solutions or protein aggregation are studied, or it can be a consequence of impurities or deterioration of the sample. In the first case, the polydispersity itself is often an object of interest, whereas in the second case it is an obstacle. In both instances, polydispersity complicates data analysis significantly.

For polydisperse solutions, Eq. (4) for the normalized field correlation function must be replaced with

$$|g^{(1)}(\tau)| = \frac{1}{I_0}\sum_i I_i \exp(-D_i q^2 \tau) \tag{9}$$

In this expression, D_i is the diffusion coefficient of particles of the ith kind and I_i is the intensity of light scattered by all of these particles. $I_i = N_i I_{0,i}$, where N_i is the number of particles of ith kind in the scattering volume and $I_{0,i}$ is the intensity of the light scattered by each such particle. For a continuous distribution of scattering particle size, Eq. (9) is generalized as

$$|g^{(1)}(\tau)| = \frac{1}{I_0}\int I(D)\exp(-Dq^2\tau)dD \tag{10}$$

Here $I(D)dD \equiv N(D)I_0(D)dD$ is the intensity of light scattered by particles having their diffusion coefficient in interval $[D, D + dD]$, $N(D)dD$ is the number of these particles in the scattering volume, and $I_0(D)$ is the intensity of light scattered by each of them. The goal of the mathematical analysis of QLS data is to reconstruct as precisely as possible the distribution function $I(D)$ [or $N(D)$] from the experimentally measured function $G^{(2)}_{\exp}(\tau)$.

It should be noted that polydispersity is not the only source of nonsingle exponential correlation functions of scattered light. Even in perfectly monodisperse solutions, interparticle interactions, orientation dynamics of asymmetric particles, and conformational dynamics or deformations of flexible particles will lead to a much more complicated correlation function than described by Eq. (4). These effects are usually insignificant for scattering by particles small compared to the length of the inverse scattering vector q^{-1}, but become important, and often overwhelming, for larger particles. In those cases, QLS probes not the pure diffusive Brownian motion of the scatterers, but also other types of dynamic fluctuation in the solution. Fortunately, the relaxation times of these other types of fluctuations rarely depend on the scattering vector as Dq^2, which is characteristic for the diffusion process. Thus, in principle, measurement of the correlation func-

tion at several different angles of scattering, and therefore at several different q, allows polydispersity to be distinguished from multimodal relaxation of a nondiffusive nature.

Deconvolution of Correlation Function, an "Ill-Posed" Problem

The values of $G^{(2)}_{\text{exp}}(\tau)$ contain statistical errors. We have described previously the features of the QLS instrument that are essential for minimizing these errors. It is equally important to minimize the distorting effect that experimental errors in $G^{(2)}_{\text{exp}}(\tau)$ have on the reconstructed distribution function $I(D)$. The distribution $I(D)$ is a nonnegative function. *A priori* then, a nonnegative function $I(D)$ should be sought that produces, via Eqs. (3) and (10), the function $G^{(2)}_{\text{theor}}(\tau)$, which is the best fit to experimental data. Unfortunately, this simplistic approach does not work. The underlying reason is that the corresponding mathematical minimization problem is "ill-posed,"[11] meaning that dramatically different distributions $I(D)$ lead to nearly identical correlation functions of the scattered light and therefore are equally acceptable fits to experimental data. For example, addition of a fast oscillating component to the distribution function $I(D)$ does not change $G^{(2)}_{\text{theor}}(\tau)$ considerably, as the contributions from closely spaced positive and negative spikes in the particle distribution cancel each other. Three approaches for dealing with this ill-posed problem are discussed.

Direct Fit Method

The simplest approach is the direct fit method. Here the functional form of $I(D)$ is assumed *a priori* (single modal, bimodal, Gaussian, etc.). The parameters of the assumed function that lead to the best fit of $G^{(2)}_{\text{theor}}(\tau)$ to $G^{(2)}_{\text{exp}}(\tau)$ are then determined. This method is only as good as the original guess of the functional form of $I(D)$. Moreover, using the method can be misleading because it may confirm nearly any *a priori* assumption made. It is also important to note that the more parameters there are in the assumed functional form of $I(D)$, the better experimental data can be fit but the less meaningful the values of the fitting parameters become. In practice, typical QLS data allow reliable determination of about three independent parameters of the size distribution of the scattering particles.

Method of Cumulants

The second approach is not to attempt to reconstruct the shape of the scattering particle distribution but instead to focus on so-called "stable"

[11] A. N. Tikhonov and V. Y. Arsenin, "Solution of Ill-Posed Problems." Halsted Press, Washington, 1977.

characteristics of the distribution, i.e., characteristics that are insensitive to possible fast oscillations. In particular, these stable characteristics are moments of the distribution or closely related quantities called cumulants.[12] The first cumulant (moment) of the distribution $I(D)$, the average diffusion coefficient $\overline{D}$, can be determined from the initial slope of the field correlation function. Indeed, using Eq. (10), it is straightforward to show that

$$-\frac{d}{d\tau}\ln|g^{(1)}(\tau)|_{\tau\to 0} = \frac{1}{I_0}\int I(D)Dq^2 dD \equiv \overline{D}q^2 \tag{11}$$

The second cumulant (moment) of the distribution can be obtained from the curvature (second derivative) of the initial part of the correlation function. As in the direct fit method, the accuracy of the real QLS experiment allows determination of at most three moments of the distribution $I(D)$. The first moment, $\overline{D}$, can be determined with better than $\pm 1\%$ accuracy. The second moment, the width of the distribution, can be determined with an accuracy of ± 5–10%. The third moment, which characterizes the asymmetry of the distribution, usually can be estimated with an accuracy of only about $\pm 100\%$.

Regularization

The regularization approach combines the best features of both of the previous methods. The advantage of the cumulant method is that it is completely free from bias introduced by *a priori* assumptions about the shape of $I(D)$, assumptions that are at the heart of the direct fit method. However, reliable *a priori* information on the shape of the distribution function, in addition to experimental data, improves the quality of results obtained by the QLS method significantly. The regularization method assumes that the distribution $I(D)$ is a smooth function and seeks a nonnegative distribution producing the best fit to experimental data. As discussed earlier, the ill-posed nature of the deconvolution problem means that distributions differing by the presence or absence of a fast oscillating function produce very similar correlation functions. The regularization requirement that the distribution should be sufficiently smooth eliminates this ambiguity, allowing unique solutions to the minimization problem. There are several methods that utilize this approach for reconstructing the scattering particle distribution function from QLS data. All of these methods impose the condition of smoothness on the distribution $I(D)$ but differ in the specific mathematical approaches used for this purpose. The most popular program,

[12] D. E. Koppel, *J. Chem. Phys.* **57**, 4814 (1972).

originally developed by Provencher,[13] is called CONTIN. We have developed and used our own algorithm.[14]

All regularization algorithms produce similar results and incorporate the use of a parameter that determines how smooth the distribution has to be. The choice of this parameter is one of the most difficult and important parts of the regularization method. If the smoothing is too strong, the distribution will be very stable but will lack details. If the smoothing is too weak, false spikes can appear in the distribution. The "rule of thumb" is that the smoothing parameter should be just sufficient to provide stable, reproducible results in repetitive measurements of the same correlation function. Two facts are helpful for choosing the appropriate smoothing parameter. First, the lower the statistical errors of the measurements, the smaller the smoothing parameter can be without loss of stability. This will yield finer resolution in the reconstructed distribution $I(D)$. Second, narrow distributions generally require much less smoothing and can be reconstructed much better than wide distributions. This is because oscillations in narrow distributions are effectively suppressed by nonnegativity conditions.

The moments of the distribution reconstructed by the regularization procedure coincide closely with those obtained by other methods. However, the regularization procedure, in addition, gives unbiased (apart from smoothing) information on the shape of the distribution. This shape cannot be extracted through use of the direct fit method or from cumulant analysis. In a typical QLS experiment, regularization analysis can resolve a bimodal distribution with two narrow peaks of equal intensity if the diffusion coefficients corresponding to these peaks differ by more than a factor of ~2.5.

Unique Features of QLS Monitoring of Fibril Growth

Effect of Fibril Length

The study of protein fibrils using QLS requires very careful interpretation of data. As fibrils grow in length, three important factors come into play. First, when the length of the fibril becomes comparable to q^{-1}, the time of diffusion of the fibril over distance Δx in the direction of vector $\mathbf{q}$, such that $q\Delta x \approx 1$, becomes dependent on the orientation of the fibril relative to this direction. As a result, even a monodisperse distribution of such fibrils will produce a multiexponential correlation function. In addition, because the intensity of the scattering by each fibril also depends on its

[13] S. W. Provencher, *Comput. Phys. Commun.* **27,** 213 (1982).

[14] T. G. Braginskaya, P. D. Dobitchin, M. A. Ivanova, V. V. Klyubin, A. V. Lomakin, V. A. Noskin, G. E. Shmelev, and S. P. Tolpina, *Phys. Scripta* **28,** 73 (1983).

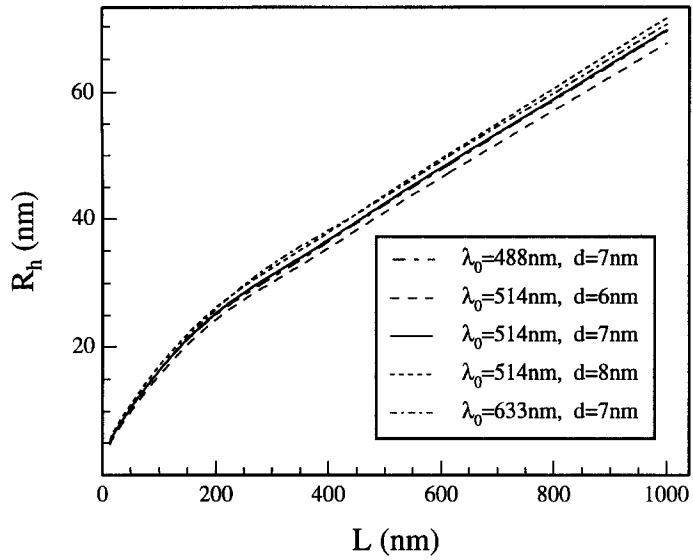

FIG. 3. Calibration curve relating R_h of a rigid rod to the rod length L. Data are shown for rod diameters of 6, 7, and 8 nm and for scattering vectors corresponding to 90° scattering in aqueous solutions with incident light of wavelength 488, 514, or 633 nm. Adapted from A. Lomakin, D. B. Teplow, D. A. Kirschner, and G. B. Benedek, *Proc. Natl. Acad. Sci. U.S.A.* **94,** 7942 (1997). Copyright (1997) National Academy of Sciences, U.S.A.

orientation relative to $\mathbf{q}$, the orientational diffusion of the fibril makes a significant contribution to the correlation function. Nevertheless, in most instances, all these effects can be subsumed into the definition of the apparent hydrodynamic radius, R_h^{app}, of the fibril. In this definition, the inverse average relaxation time of the multiexponential correlation function given by the left side of Eq. (11) is used to calculate the apparent diffusion coefficient, D^{app}, which is then used in Eq. (6) to calculate R_h^{app}. Figure 3 presents numerically calculated curves of $R_h^{app}(L)$ for several different q. Using data in Fig. 3, fibril length can be determined from the value of R_h^{app}. It should be noted that when L remains relatively small, $R_h^{app}(L)$ is insensitive to variations in wavelength and fibril diameter.

Effect of Fibril Flexibility

When the length of the fibril becomes comparable to the persistence length,[15] the effects of fibril flexibility must be taken into account. Flexibility adds even more complexity to the anisotropic diffusion and orientational

[15] O. Kratky and G. Parod, *Rec. Trav. Chim.* **68,** 1106 (1949).

dynamics of a fibril. Effects of flexibility on the correlation function have been discussed in detail by Maeda and Fujume.[16,17] For the same length, a flexible fibril will have a smaller R_h^{app} than a rigid one. Fibrils that are much longer than the persistence length l_p form coils with apparent hydrodynamic radii of $(3\sqrt{\pi}/8)R_g$, where $R_g = \sqrt{2Ll_p}$ is the radius of gyration of the coil and L is the contour length of the fibril. This is a much weaker dependence on $R_h^{app}(L)$ than that for rigid rods [Eq. (8)]. If, in addition, the radius of gyration is large compared to q^{-1}, the correlation function of the scattered light is then determined by the diffusion of the segment of the coil of size q^{-1} and becomes independent of the total fibril length.

Effect of Fibril–Fibril Interaction

The third, and potentially most serious, factor affecting the interpretation of QLS data on growing fibrils is fibril–fibril interaction. Even in the absence of attraction between fibrils, fibril–fibril interactions become significant in what is known as the "semidilute" concentration regime. This regime occurs when fibrils grow sufficiently long so that average fibril length becomes comparable to or longer than the average distance between fibrils. Let us consider fibrils of diameter d and average fibril length L occupying volume fraction ϕ of the solution. The volume of an individual fibril is $v \sim d^2L$ and the number N of fibrils in a unit volume is $N = \phi/v$. The average distance between fibrils is $N^{-1/3}$. The semidilute regime starts when $N^{-1/3} \sim L$, and, therefore, $L^3 = Ld^2/\phi$. From these estimates, it is clear that fibril–fibril interactions become important when fibrils reach the length L^*, which is related to fibril diameter by the following equation:

$$L^* = d/\sqrt{\phi} \tag{12}$$

Regardless of the concentration, sufficiently long rigid fibrils always enter the semidilute regime. In a semidilute solution, fibrils cannot move perpendicular to their long axes because of caging by other fibrils. They only diffuse along their axes.[18] The dynamic behavior of semidilute solutions of rods has been discussed by Zero and Pecora[19] and reviewed thoughtfully by Russo.[20] Qualitatively, fibril–fibril interaction in a semidilute solution

[16] T. Maeda and S. Fujume, *Macromolecules* **17,** 1157 (1984).
[17] T. Maeda and S. Fujume, *Macromolecules* **17,** 2381 (1984).
[18] M. Doi and S. F. Edwards, *J. Chem. Soc. Faraday II* **74,** 569 (1978).
[19] K. Zero and R. Pecora, *in* "Dynamic Light Scattering: Applications of Photon Correlation Spectroscopy" (R. Pecora, ed.), p. 59. Plenum Press, New York, 1985.
[20] P. S. Russo, *in* "Dynamic Light Scattering" (W. Brown, ed.), p. 512. Claredon Press, Oxford, 1993.

slows down the diffusion of fibrils dramatically and, if unaccounted for, leads to gross overestimation of fibril length.

Practical Aspects of QLS Experiments

Temperature Control

The diffusion coefficient D depends on the temperature T both explicitly and through the solvent viscosity η. In aqueous solutions, this dependency is strong. Indeed, near room temperature, the factor T/η in the Stokes–Einstein relation between D and R [Eq. (5)] changes ~3% per 1°. To obtain consistent results, it is thus essential to stabilize the temperature of the sample precisely. It is also important to avoid local heating of the sample by the focused laser beam, which if unaccounted for can cause systematic underestimation of the size of the scattering particles. In addition, local heating can cause convection and thermal lens effects, which can affect the quality of the QLS measurements adversely. The degree of local heating depends on light absorption by the sample solution. In most cases, if the intensity of the laser is adjusted so that several photocounts per coherence area per correlation time are produced, overheating of the scattering volume is rarely a problem.

Laser Modes and Stability

In QLS experiments, the laser must operate in the single mode regime, i.e., it should generate a single transverse mode (called TEM_{00}). Different transverse modes have different cross-sectional intensity profiles and very close frequencies. The mode TEM_{00} produces a beam with a nearly Gaussian intensity profile. If the laser were to generate several transverse modes simultaneously, not only would the beam have an irregular intensity profile, but more importantly, optical "beating" between these modes would be registered by the photodetector. This would result in significant distortion of the correlation function.

Laser stability is another requirement for successful QLS experimentation. Fluctuations of laser intensity can be caused by mechanical vibration, thermal expansion, and fluctuations in power supply performance. Depending on their origin, intensity fluctuations of the incident beam can occur as oscillations, large abrupt changes due to "mode hops," or slow drifting of intensity. To account for the fluctuations in laser intensity, the factor I_0^2 in the expression for the intensity correlation function $G^2(\tau)$ in Eq. (3) should be replaced by the correlation function of the laser intensity, $\langle I_0(0) \cdot I_0(t) \rangle = I_0^2 + \langle \delta I(0) \cdot \delta I(\tau) \rangle$. Here $\delta I(t)$ is the deviation of the laser

intensity at moment t from its average value I_0. From examination of Eq. (3), we see that with a low efficiency factor γ, even small fluctuations in laser intensity can have significant effects on the determination of $|g^1(\tau)|$. It is therefore important to use a well-stabilized laser and to maximize the efficiency of measurements by collecting light from a single coherence area. If mode hops happen during the measurements, $\delta I \sim I_0$. In this case, the resulting data should be discarded.

Sample Purity

Samples monitored by QLS must be optically pure. This concept is quite different from the concept of chemical purity. In the latter case, one or a few large inert particles would not be expected to affect the phenomenon under study. However, in the case of QLS, the fact that the intensity of light scattered by a particle is proportional to the square of the particle mass (for particles small compared to the wavelength of the incident light) means that even a small weight fraction of large scatterers can completely dominate scattering from a population of relatively small particles. A common problem associated with monitoring protein assembly processes is the presence of very large particles, such as dust particles and protein aggregates. These particles occasionally drift inside the scattering volume, increasing the total scattering intensity several times. This is as detrimental to the QLS experiment as are mode hops and can make QLS measurements unusable.

Three approaches are commonly used to deal with large, biologically irrelevant particles: *pre facto* particle removal, careful control of the illuminated sample volume, and *post facto* data manipulation. The easiest way to remove large impurities from solution is by filtration. Standard 0.22-μm filters generally are too porous to be of use. We have found that 20-nm Anatop filters are satisfactory. In cases where the particles of interest are too big to pass through the 20-nm filter, their scattering intensity is usually great enough so that dust and other large particles do not significantly corrupt the resulting data set. It should be noted that dust in the air has a strong tendency to adsorb electrostatically to charged groups on the surfaces of the empty cuvette. These adsorbed particles can be suspended in the sample solution during the process of expulsion of the sample from the filter. If the cuvette is not to be filled completely, it is desirable to introduce the sample into the bottom of the cuvette to avoid washing dust off the cuvette walls. This is typically done by first sealing the cuvette with Parafilm, attaching a narrow gauge needle to the filter bottom, piercing the Parafilm seal with the needle, and positioning the needle tip at the cuvette bottom.

Centrifugation is another effective way to remove large impurities from the solution, provided that the sample is spun in the same sealed cuvette in which the QLS measurements will be done. Transferring the sample into another cuvette after centrifugation defeats the purpose of the procedure. Typical airborne dust can be pelleted in 30 min at 5000*g*. However, there are always very "flaky" dust particles that will not sediment by this procedure.

Successful measurement of the hydrodynamic radius of low molecular weight molecules is absolutely dependent on the optical purity of the sample. In studies of the amyloid β-protein, we have used the intrinsic filtering potential of high-performance liquid chromatography (HPLC) column packings, and a continuous flow procedure for washing the QLS cuvette, to produce optically pure Aβ samples. We first prepared cuvettes by heating the top 20 mm of standard 6 × 50-mm glass test tubes in the flame of a small torch. The tops of each tube are then pulled to form narrow capillaries. A similar procedure is performed on disposable glass micropipettes in order to form a junction between the HPLC detector and the cuvette. In this case, the untreated end of the micropipette is inserted into the HPLC detector outflow line while the pulled tip of the micropipette is inserted into the cuvette so that its tip is at the very bottom. In this way, "filtered" buffer is constantly washing the interior of the cuvette from the bottom out through the narrow capillary top. When the peak of interest has passed the detector and filled the cuvette, the micropipette is removed from the cuvette and the end of the cuvette is immediately fire sealed. This procedure, although somewhat cumbersome, provides excellent dust-free samples. We strongly recommend it for any QLS study of peptides and small proteins.

The second approach for dealing with large particles involves careful focusing of the laser beam in order to minimize the scattering volume. Dust particles or aggregates pass through a small scattering volume less frequently and in fewer numbers than through larger volumes. In addition, high brightness of the beam improves the signal-to-noise ratio, allowing collection of the light from fewer coherence areas. This increases the value of the important efficiency factor γ in Eq. (3).

Despite diligent efforts to produce optically pure samples and a well-focused beam, large particles often pass through the illuminated volume. As a result, significant fluctuations in the intensity of the scattered light are produced. These fluctuation are of a different nature than the standard fluctuations in the interference pattern and are difficult to account for. Some correlators allow suppression of data acquisition during spikes of intensity. These algorithms are called "software dust filters" and involve establishing arbitrary cutoff levels for the intensity of the scattered light. In addition, large particles can be identified by data analysis software, which reconstructs particle size distributions. Thus, in principle, regularization

algorithms can alleviate the effect of dust on the reconstructed distribution of particle sizes. However, these *post facto* approaches have limited usefulness. It is thus most advantageous to minimize the effects of irrelevant large particles by removing them *pre facto*.

Assembly of Amyloid β-Protein (Aβ)

Aβ Fibrillogenesis

This section illustrates how QLS techniques may be applied to investigate protein assembly using examples from studies of the kinetics of Aβ fibrillogenesis. Aβ plays a seminal role in the pathogenesis of Alzheimer's disease, during which this peptide accumulates as amyloid deposits in many regions of the brain.[21] Fibrillogenesis of Aβ is associated with neuronal damage, thus efforts directed at inhibiting or reversing this process could have therapeutic value. An elucidation of the morphologic and kinetic stages of fibrillogenesis would permit thoughtful targeting and design of therapeutic agents.[22] As a step toward understanding the molecular mechanism of Aβ fibrillogenesis, we have used QLS to monitor quantitatively the temporal evolution of the fibril length distribution in solutions of synthetic Aβ *in vitro*.

It should be emphasized that the ability to monitor quantitatively the fibril length distribution allows determination of the rate constants for fibril nucleation and elongation, k_n and k_e, respectively.[23,24] Knowledge of these quantities is sufficient to model the fibrillogenesis process in a given system. Importantly, examination of the effects of perturbations of the system on these kinetic parameters can provide data about key elements controlling the fibrillogenesis process. The following examples demonstrate how the QLS approach has been used to determine rate constants for Aβ fibrillogenesis,[23,24] to examine the type of macromolecular assemblies formed during Aβ polymerization,[25] to determine the effects of primary structure

[21] D. J. Selkoe, *Science* **275,** 630 (1997).
[22] D. B. Teplow, *Amyloid Int. J. Exp. Clin. Invest.* **5,** 121 (1998).
[23] A. Lomakin, D. S. Chung, G. B. Benedek, D. A. Kirschner, and D. B. Teplow, *Proc. Natl. Acad. Sci. U.S.A.* **93,** 1125 (1996).
[24] A. Lomakin, D. B. Teplow, D. A. Kirschner, and G. B. Benedek, *Proc. Natl. Acad. Sci. U.S.A.* **94,** 7942 (1997).
[25] D. M. Walsh, A. Lomakin, G. B. Benedek, M. M. Condron, and D. B. Teplow, *J. Biol. Chem.* **272,** 22364 (1997).

changes on fibrillogenesis kinetics,[26] and to elucidate thermodynamic properties of the fibrillogenesis reaction.[27]

Quantitative Monitoring of Earliest Stages of Fibrillogenesis

Aβ fibrils have diameters $d \approx 6$–10 nm and have linear densities $\rho \approx 1.6$ nm^{-1}.[23,28] At a total Aβ concentration $C = 0.1$ mM, a solution of Aβ fibrils occupies a volume fraction $\phi = CN_A\pi d^2/4\rho \approx 2 \times 10^{-3}$, where N_A is Avogadro's number and d is fibril diameter (in this case 8 nm). According to Eq. (12), the transition to the semidilute regime in this solution starts when fibrils are approximately 150 nm long. This length is close to the estimated persistence length of Aβ fibrils[29] and to the typical value of $\sim$100 nm for q^{-1}. These values mean that the quantitative analysis of fibril assembly by QLS is most appropriate when fibril length does not exceed 100–150 nm. The QLS method is thus ideal for examining the critical early stages of fibril assembly, i.e., the nucleation and elongation of nascent fibrils. Among the methods used to monitor Aβ fibrillogenesis, which include Congo red and thioflavin T binding, turbidimetry, sedimentation, filtration, atomic force microscopy, and electron microscopy, only QLS can provide directly an absolute, quantitative measure of Aβ particle size during fibril nucleation and elongation. At later stages, when solutions contain longer fibrils, structural information can still be obtained, but it is more qualitative in nature.

Measurement of Fibril Elongation Rates

By relating R_H^{app} to L, QLS can be used to determine temporal changes in fibril length, i.e., the elongation rate dL/dt. This is an extremely powerful capability because it enables the mechanistic study of fibril elongation. Determination of the concentration dependence of dL/dt is one method for studying the mechanism of polymer elongation reactions. The elongation rate and the rate of monomer addition at the fibril tip, dN/dt, are related by the equation $dN/dt = \rho dL/dt$, where ρ is the linear density of monomers

[26] D. B. Teplow, A. Lomakin, G. B. Benedek, D. A. Kirschner, and D. M. Walsh, *in* "Alzheimer's Disease: Biology, Diagnosis and Therapeutics" (K. Iqbal, B. Winblad, T. Nishimura, M. Takeda, and H. M. Wisniewski, eds.), p. 311. Wiley, Chichester, England, 1997.

[27] Y. Kusumoto, A. Lomakin, D. B. Teplow, and G. B. Benedek, *Proc. Natl. Acad. Sci. U.S.A.* **95,** 12277 (1998).

[28] C. L. Shen, M. C. Fitzgerald, and R. M. Murphy, *Biophys. J.* **67,** 1238 (1994).

[29] C. L. Shen and R. M. Murphy, *Biophys. J.* **69,** 640 (1995).

within the fibril. To determine dL/dt, the slope of the curve $L(t)$ is measured when the most reliable connection between R_h^{app} and L exists, i.e., during the initial nucleation and elongation of fibrils when $L \leq 150$ nm. To do so, $L(t)$ is reconstructed from the time dependency of the apparent R_h, which in turn is derived from $D^{app}(t)$ according to Eq. (6). This process is illustrated in the following example, in which temporal changes in the distribution of apparent diffusion coefficients D^{app} were measured during the fibrillogenesis of Aβ(1–40), one of the two major forms of the peptide found in amyloid deposits *in vivo*.[22] This approach resulted in the discovery of a novel mechanism for Aβ fibril nucleation, namely nucleation within Aβ micelles.[23]

The experiment is performed by dissolving HPLC-purified Aβ(1–40)

[*NH_2*-DAEFRHDSGYEVHHQKLVFFAED
VGSNKGAIIGLMVGGVV-*COOH*]

at concentrations ranging from 25 μM to 1.7 mM in 0.1 N HCl. For each concentration, ~200 μl of sample is placed in a 5-mm-diameter glass test tube and then centrifuged at 5000g for 30 min to pellet dust particles and large aggregates. The tube is then placed into the QLS spectrometer, and the intensity and correlation function of the scattered light are measured periodically over the next 20–50 hr. Each measurement lasts 5–30 min, depending on the intensity of the signal. During the monitoring period, the sample remains at ~22°. Figure 4A shows distributions of D^{app} during fibrillogenesis of Aβ(1–40) at a total concentration $C_0 = 0.25$ mM. Initially, the distributions are unimodal and narrow (data not shown), reflecting the presence of a relatively homogeneous population of scattering particles with large diffusion coefficients. Within 1–2 hr, an asymmetry develops in the distribution, characteristic of the presence of larger particles (Fig. 4A, 1.7 hr). As time passes, a bimodal distribution develops in which the population of larger scatterers displays a decreasing apparent diffusion coefficient. Finally, the more rapidly diffusing particles disappear, at which point the distribution of large particles becomes fixed (data not shown).

Using Eq. (6), $R_h^{app}(t)$ can be derived for each concentration C_0. Applying this process to data of Fig. 4A yields Fig. 4B. Here we see that the rapidly diffusing scatterers have an R_h = 5–7 nm,whereas the R_h distribution of the larger particles emerges from that of the smaller and displays a temporally increasing mean value and intensity. By averaging across the entire distribution, one obtains the mean hydrodynamic radius, $\overline{R_h}$. The time dependence of $\overline{R_h}$ is shown in Fig. 5. The initial $\overline{R_h}$ for each C_0, determined by extrapolation of the linear portion of each growth curve to $t = 0$, is 4 nm. This value is concentration independent. However, for $C_0 > 0.1$ mM, especially at higher concentrations, an apparent lag phase

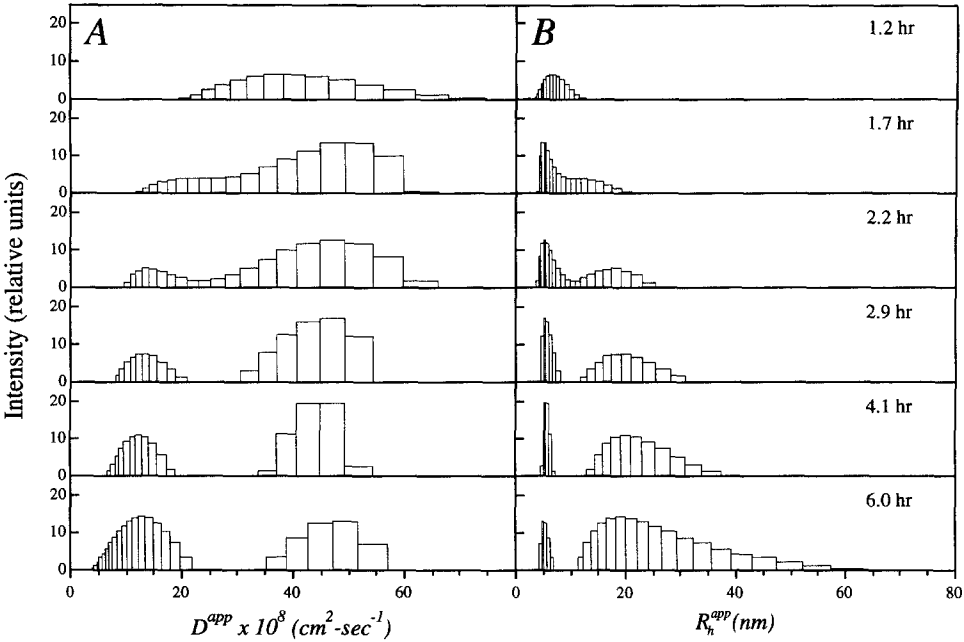

FIG. 4. Temporal evolution of the distribution of apparent diffusion coefficients (A) and apparent hydrodynamic radii (B) during fibrillogenesis of Aβ(1–40).

is observed during which time $\overline{R_h}$ remains constant at ~7 nm. Using the numerical relationship between R_h^{app} and L shown in Fig. 3, curves of $L(t)$ are constructed for each concentration of Aβ examined. Determination of the initial slopes of these curves yielded values for dL/dt (Fig. 6) and enabled assessment of the concentration dependence of the initial elongation rate. Interestingly, the kinetics differ depending on whether C_0 is above or below ~0.1 mM. We refer to this concentration as the critical concentration c^*. Below this concentration, initial rates of fibril elongation are proportional to C_0, but above this concentration, the fibrillogenesis kinetics is concentration independent. In fact, over a full decade of concentrations above c^* (0.17–1.7 mM), experimental measurements of $\overline{R_h}(t)$ yielded essentially the same results (Fig. 5). The concentration 0.1 mM thus constitutes a boundary above and below which very different fibrillogenesis behavior occurs. The final fibril length, L_f, also shows a different concentration dependence above and below c^* (Fig. 6). For $C_0 < c^*$, L_f is related inversely to concentration. However, for $C_0 > c^*$, L_f is independent of concentration and is significantly lower than the final average L_f values observed in experiments done at $C_0 < c^*$.

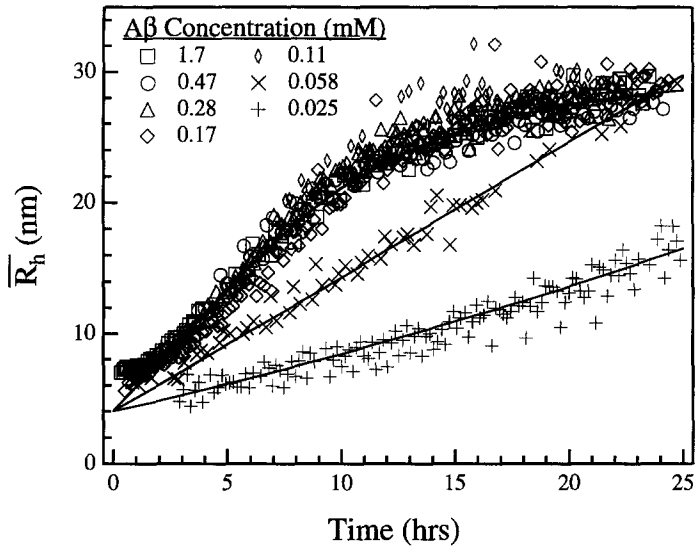

FIG. 5. Concentration dependence of Aβ fibrillogenesis. Solid lines have been drawn through data to assist the eye. Adapted from A. Lomakin, D. S. Chung, G. B. Benedek, D. A. Kirschner, and D. B. Teplow, *Proc. Natl. Acad. Sci. U.S.A.* **93,** 1125 (1996). Copyright (1996) National Academy of Sciences, U.S.A.

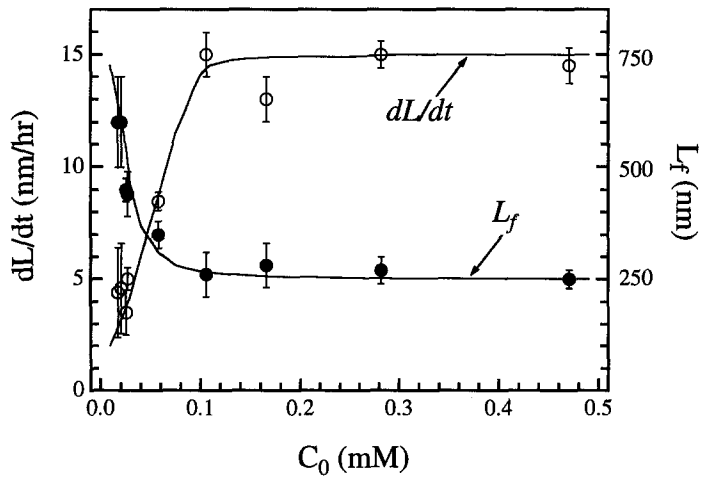

FIG. 6. Concentration dependence of fibril elongation rate (dL/dt) and final fibril length (L_f). Adapted from A. Lomakin, D. S. Chung, G. B. Benedek, D. A. Kirschner, and D. B. Teplow, *Proc. Natl. Acad. Sci. U.S.A.* **93,** 1125 (1996). Copyright (1996) National Academy of Sciences, U.S.A.

These observations formed the basis for development of a model of Aβ fibril nucleation and elongation in which micellization occurs in the concentration domain $C_0 > c^*$.[23] Micelles are the 7-nm particles seen immediately on peptide dissolution and are nidi for Aβ fibril nucleation. Nascent nuclei, the 4-nm particles seen in all experiments, are then extended by Aβ monomer addition at their ends. A full mathematical formulation of this model has been published.[24] Importantly, this formulation provides values for the key kinetic rate constants of the model, nucleation rate k_n and elongation rate k_e. It also enables determination of the time-dependent changes in monomer and micelle concentration and in the concentration and size distribution of fibrils as fibrillogenesis proceeds. The ability to monitor quantitatively the earliest nucleation and elongation events occurring during Aβ fibrillogenesis is a unique and particularly powerful characteristic of QLS.

Simultaneous Monitoring of Intensity and Hydrodynamic Radius Discriminates between Fibrillogenesis and Amorphous Aggregation

As shown earlier, the intensity of the light scattered by a single small particle composed of m monomers is $I = m^2 I_0$. In a monodisperse system of n scatterers, the total intensity of the scattered light would be simply $I = nm^2 I_0$. In a closed system, the total number of monomers $M = nm$ remains constant and thus aggregation is characterized by a proportionality between scatterer size and scattered light intensity, i.e., $I = MmI_0$. In polydisperse systems, m should be replaced with the weight-averaged aggregation number of the scatterers.

The hydrodynamic radius of an aggregate depends on its geometry. For a dense spherical particle, $R_h \sim m^{1/3}$. For thin rigid rods, their length is proportional to monomer number, i.e., $L \sim m$, and Eq. (8) shows that R_h increases nearly proportionally to the size of aggregate. Therefore, for linear elongation, normalized curves of the temporal change in R_h and I will be similar, whereas amorphous and other types of nonlinear aggregation produce a disproportionate increase in I relative to R_h. This is illustrated in Fig. 7, where the temporal changes in $\overline{R_h}$ and intensity observed during fibrillogenesis of wild-type Aβ(1–40) and of a mutant Aβ molecule associated with amyloidosis in a Dutch kindred are plotted.[30] Here, the wild-type molecule displays a proportionality between R_h and I as fibrils grow. In contrast, during the period from 5 to 30 hr, the "Dutch" peptide displays a fourfold increase in I whereas $\overline{R_h}$ increases <50%. This is consistent with fibril–fibril bundling of the Dutch peptide.

[30] E. Levy, M. D. Carman, I. J. Fernandez-Madrid, M. D. Power, I,. Lieberburg, S. G. van Duinen, G. T. A. M. Bots, W. Luyendijk, and B. Frangione, *Science* **248,** 1124 (1990).

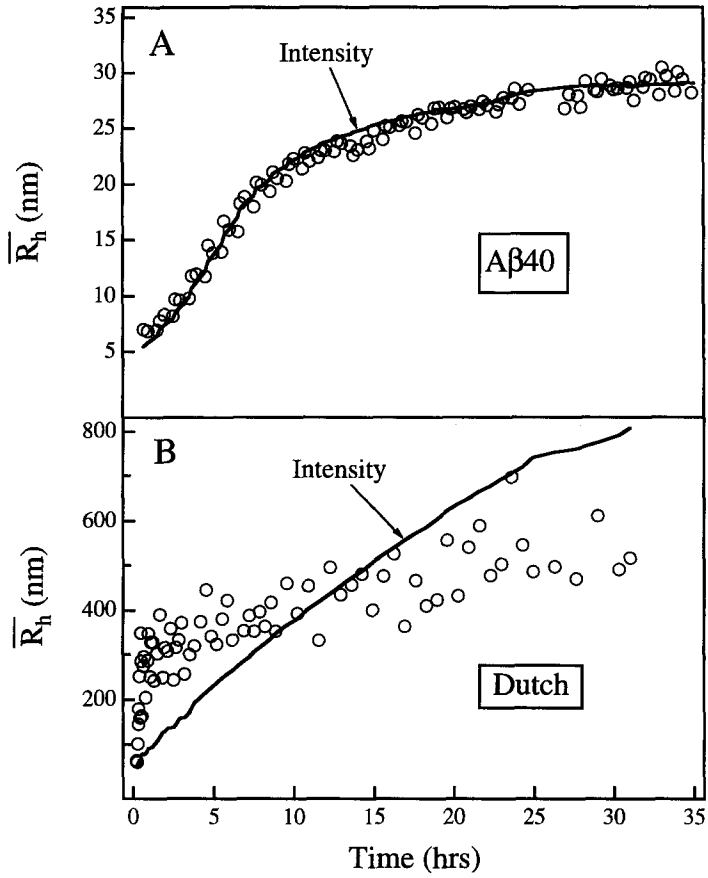

FIG. 7. Temporal changes in $\overline{R_h}$ and scaled intensity observed during fibrillogenesis of wild-type Aβ (A) and Dutch Aβ (B). Adapted from D. B. Teplow, *in* "Molecular Biology of Alzheimer's Disease: Genes and Mechanisms Involved in Amyloid Generation" (C. Haass, ed.), p. 163. Harwood Academic, Amsterdam, 1998.

The just-described considerations relating I and $\overline{R_h}$ are valid only while aggregates remain small compared to q^{-1}. As soon as aggregate size exceeds this value, no further increase of intensity will be observed. In addition, the relationship between $\overline{R_h}$ and intensity is not that straightforward in a polydisperse system. With these caveats in mind, it is nevertheless valuable to recognize that out of all possible aggregates of a given mass, linear rods have the smallest intensity of scattering and the largest $\overline{R_h}$. Thus, linear fibrillization produces the least possible increase of intensity of scattering as a function of $\overline{R_h}$.

Effects of Primary Structure Changes on Nucleation and Elongation Rates

The Dutch mutation mentioned earlier causes a $Glu^{22} \rightarrow Gln$ amino acid substitution within the Aβ sequence, which leads to severe amyloid deposition within cerebral blood vessels, resulting in fatal strokes. In an effort to correlate this neuropathology with the biophysical behavior of the mutant peptide, the kinetics of fibrillogenesis of the Dutch peptide was studied using QLS.[26] The peptide was dissolved at a concentration of 0.1 m*M* in 0.1 *N* HCl at room temperature and the temporal change in $\overline{R_h}$ and in the average intensity of the scattered light were measured. Relative to wild-type Aβ, a 200-fold increase in initial elongation rate was observed (Fig. 8). Furthermore, an 8-fold increase in final fibril length was seen. In the concentration domain $C_0 > c^*$, the final fibril size is given by the equation $L_f = (k_e c^*/k_n)^{1/2}/\rho$.[23] The ratio of nucleation rates therefore can be estimated as $k_n^{Dutch}/k_n^{wild\ type} \approx 3$. This demonstrates that the $Glu^{22} \rightarrow$ Gln mutation accelerates both nucleation and elongation of fibrils. The ability to quantify differences in nucleation and elongation rates provides the means to identify key structures, such as Glu^{22} in Aβ, controlling the kinetics of protein assembly reactions.

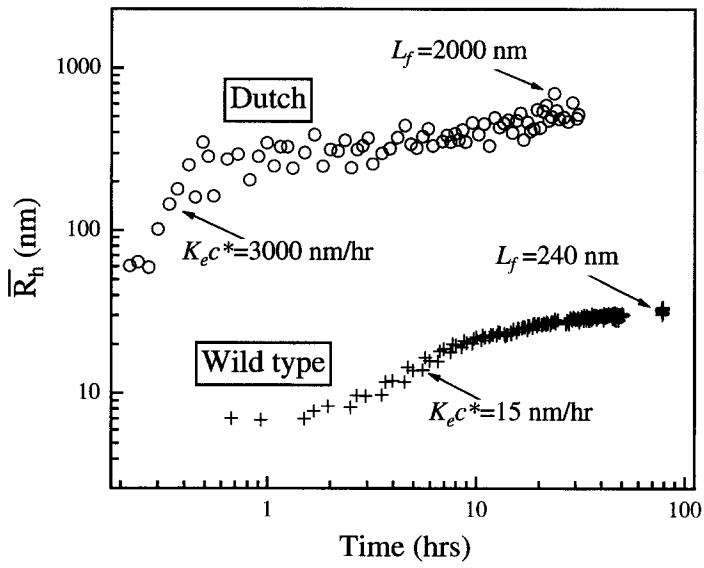

FIG. 8. Effect of the Dutch amino acid substitution on the kinetics of Aβ fibrillogenesis (note the log scales). Adapted from D. B. Teplow, *in* "Molecular Biology of Alzheimer's Disease: Genes and Mechanisms Involved in Amyloid Generation" (C. Haass, ed.), p. 163. Harwood Academic, Amsterdam, 1998.

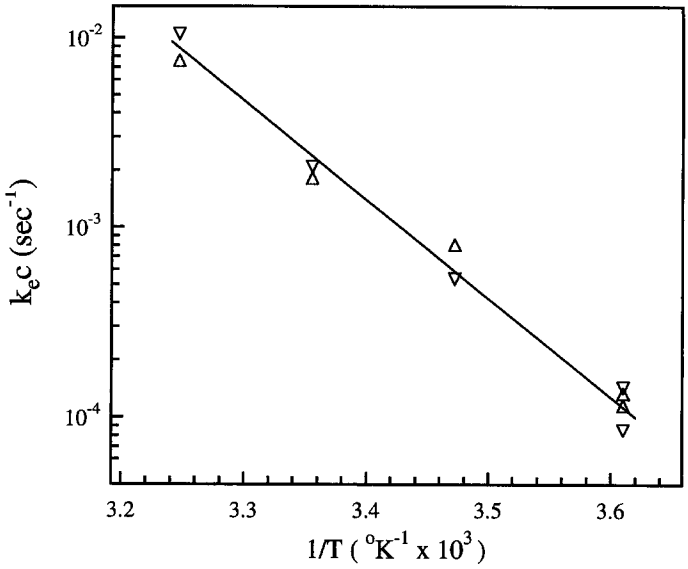

FIG. 9. Arrhenius plot of initial fibril elongation rate versus inverse temperature. Two sets of samples (▽, △) were prepared and their elongation rates were determined in 0.1 *N* HCl at four different temperatures. Resulting data were fit well by a straight line ($r = -0.99$) whose slope yielded an activation energy E_A = 22.8 kcal/mol. Adapted from Y. Kusumoto, A. Lomakin, D. B. Teplow, and G. B. Benedek, *Proc. Natl. Acad. Sci. U.S.A.* **95,** 12277 (1998). Copyright (1998) National Academy of Sciences, U.S.A.

Thermodynamics of Aβ Fibrillogenesis

The QLS approach allows one to address fundamental questions about the mechanism of the fibril elongation reaction. Previous studies have shown that the temporal increase in thioflavin T binding that occurs during Aβ fibrillogenesis depends on temperature.[31] Because of their low resolution, dye-binding approaches do not allow determination of whether the temperature dependence exhibited is due to the fibril elongation reaction, fibril–fibril association, or other processes. We therefore used QLS to study the temperature dependence of Aβ fibrillogenesis quantitatively. We determined the fibril elongation rate k_e in a series of experiments in which Aβ(1–40) was allowed to fibrillize at temperatures ranging from 4 to 40°. In each case, we could show that the function $k_e(T)$ obeyed the Arrhenius relationship $k_e = A \exp(-E_A/kT)$, where A is a preexponential constant and E_A is the activation energy for the reaction (Fig. 9).[27] Using this relationship, and examining the monomer addition reaction in the context of transi-

[31] H. Naiki and K. Nakakuki, *Lab. Invest.* **74,** 374 (1996).

tion-state theory, one can deduce the thermodynamic characteristics of the activation process. We found that the activation energy E_A was ~23 kcal/mol and that the activation entropy ΔS was ~53 cal/mol-deg. These numbers show that the fibril elongation reaction requires a significant input of energy and involves substantial conformational changes, e.g., unfolding of Aβ at the fibril tip or increased disorder of associated solvent molecules. The activation process thus may provide targets for therapies aimed at preventing the formation of Aβ conformers involved in fibril elongation.

Summary

This article discussed the principles and practice of QLS with respect to protein assembly reactions. Particles undergoing Brownian motion in solution produce fluctuations in scattered light intensity. We have described how the temporal correlation function of these fluctuations can be measured and how mathematical analysis of the correlation function provides information about the distribution of diffusion coefficients of the particles. We have explained that deconvolution of the correlation function is an "ill-posed" problem and therefore that careful attention must be paid to the assumptions incorporated into data analysis procedures. We have shown how the Stokes–Einstein relationship can be used to convert distributions of diffusion coefficients into distributions of particle size. In the case of fibrillar polymers, this process allows direct determination of fibril length, enabling nucleation and elongation rates to be calculated. Finally, we have used examples from studies of Aβ fibrillogenesis to illustrate the power these quantitative capabilities provide for understanding the molecular mechanisms of the fibrillogenesis reaction and for guiding the development of fibrillogenesis inhibitors.

Acknowledgments

We gratefully acknowledge the critical comments provided by Drs. Dominic Walsh, Youcef Fezoui, Jayanti Pande, Neer Asherie, and George Thurston. This work was supported by Grant 1P01AG14366 from the National Institutes of Health, through the generosity of the Foundation for Neurologic Diseases, and by Amgen/MIT and Amgen/Brigham and Women's Hospital research collaboration agreements.